Adjoint-based optimization of a source-term representation of vortex generators

Florentie, Liesbeth; Hulshoff, Steven; van Zuijlen, Alexander

DOI
10.1016/j.compfluid.2017.12.009

Publication date
2017

Document Version
Final published version

Published in
Computers & Fluids

Computers and Fluids 162 (2018) 139–151

Contents lists available at ScienceDirect

Computers and Fluids

journal homepage: www.elsevier.com/locate/compfluid

Adjoint-based optimization of a source-term representation of vortex generators

Liesbeth Florentie*, Steven J. Hulshoff, Alexander H. van Zuijlen

Delft University of Technology, Kluyverweg 1, 2629 HS, Delft, The Netherlands

ARTICLE INFO

Article history:
Received 5 April 2017
Revised 30 October 2017
Accepted 15 December 2017
Available online 16 December 2017

Keywords:
Continuous adjoint method
Source-term model
Vortex generators
Finite-volume method
Computational fluid dynamics

ABSTRACT

An optimization approach is presented that can be used to find the optimal source term distribution in order to represent a high-fidelity vortex-generator (VG) induced flow field on a coarse mesh. The approach employs the continuous adjoint of the problem, from which an exact sensitivity is calculated and used in combination with a trust-region method to find the source term which minimizes the deviation with respect to the reference velocity field. The algorithm is applied to an incompressible flow over a rectangular VG and VG pair on a flat plate and compared to results obtained with the jBAY-model and a body-fitted mesh simulation. The results indicate that a highly accurate flow, yielding only minimal errors with respect to the shape factor, circulation and vortex core, can be obtained on coarse meshes when adding a source term to only a limited number of cells. This approach therefore demonstrates the potential of source-term models to include the effects of VGs in computations of large-scale geometries. It also allows quantification of the achievable accuracy on a particular mesh and the calculation of the source term which is optimal for a specific situation. Furthermore, the optimization approach can be used to diagnose the deficiencies of an existing source-term VG model, in this work the jBAY model.

1. Introduction

Flow-control devices have the capability of increasing the performance of for example wind-turbine blades, engine inlet ducts or airplane wings considerably [1,2]. One of the most commonly used tools in this respect are passive vortex generators (VGs), which consist of small vanes that are mounted on a surface of interest at an angle relative to the incoming flow. VGs introduce streamwise vortical structures that provide mixing in the inner part of the boundary layer with the high-momentum flow of the outer region, thus locally re-energizing the flow. They thereby increase the ability of the flow to overcome adverse pressure gradients and hence reduce its susceptibility to flow separation [3]. By ensuring an attached flow over a larger region of the surface, the addition of VG arrays to e.g. wind-turbine blades increases the maximum lift forces and stall angles, resulting in improved power generation and overall better performance [4–6].

However, reliable predictions of the effects of VGs, and the determination of optimal configurations for specific operating conditions, is not straightforward. These require the ability to accurately model the physics associated with the flow patterns induced by individual VGs and their combined effects when operating in arrays. Computational fluid dynamics (CFD) simulations which resolve the VG geometry could potentially offer the required fidelity, but the computational cost would be excessive, due to the large difference in scale between VGs (with a height typically smaller than the boundary-layer thickness) and the overall structure of interest.

A more feasible approach is to model the effect of the VG on the flow by the addition of a suitable source term to the governing equations. Then only minor or even no mesh adaptations are required with respect to clean-surface simulations, resulting in large savings in computational cost. For example, this can be advantageous for the determination of optimal VG locations. An overview of such source-term VG models is contained in [7]. Common approaches include the addition of a predefined vortex profile based on analytic models [8,9], either as secondary velocities or more recently as additional turbulent stresses [10]. A disadvantage of these methods is that they rely on the inherent assumption that the created vortex can be described by an analytic idealized-vortex model (often the Lamb–Oseen model), usually in combination with empirical relations. Thereby they fail to fully take into account the particular characteristics of the situation of interest, for example the VG geometry and flow conditions.

* Corresponding author.
E-mail address: l.florentie@tudelft.nl (L. Florentie).

https://doi.org/10.1016/j.compfluid.2017.12.009

An alternative consists of including body forces to the governing equations that trigger the formation of a vortex with suitable characteristics [11,12], hence making no prior assumption on the shape and strength of the final vortex. An example is the VG model proposed by Bender et al. [11] (usually referred to as the BAY model), and its improved version the jBAY model [13], which makes use of airfoil theory to estimate the lateral forces generated by the VG. Both the BAY and the jBAY models are commonly used in industry.

Analysis of the BAY and jBAY models by Florentie et al. [14] has shown that this approach performs reasonably well, creating a vortex with characteristics similar to those of a reference body-fitted mesh simulation. However, also some shortcomings are observed. It is found that still a rather refined mesh is required in the vicinity of the VGs, and that the vortex characteristics do not converge to the body-fitted mesh results upon refinement of the mesh. Moreover, analysis of the boundary-layer shape factor revealed deviations that could indicate unreliability with respect to separation prediction. Being constrained by the use of suboptimal meshes, it is unclear whether and to which extent improvement is possible. The question thus arises what is the highest accuracy one can expect to achieve when making use of a source-term model to simulate VG-induced flow effects, on a given mesh? More importantly, which source term would be able to yield this result? In this contribution we present an inverse approach to answer both questions. We perform a goal-oriented optimization, using the adjoint system, to calculate the optimal source-term distribution that recreates the characteristics of a given high-fidelity 3D flow field on a low-resolution mesh.

The formulation of this optimization problem and the derivation of the adjoint system is presented in the next section, followed by details about the numerical implementation. This is followed by an overview of the problems used to test our approach and the derivation of the corresponding boundary conditions. A discussion of the results obtained, with respect to attainable accuracy and source-term patterns, is presented in Sections 5–7.

Note that although the current work is focused on the simulation of VG-induced flow effects, the presented methodology is general. It can in theory also be used to find a suitable source term to replace other small obstacles in CFD simulations.

2. Methodology

2.1. Formulation of the optimization problem

Our objective is to find a source term that accurately reproduces the flow disturbance caused by the presence of a VG. This disturbance consists of a vortex within the boundary layer, propagating downstream and thereby altering the boundary-layer profile. Quantities of interest when analyzing this effect include the (location and value of the peak in the) vorticity field,

$$\omega = \nabla \times \mathbf{u}, \tag{1}$$

and its integral measure accounting for the change in overall flow circulation,

$$\Gamma = \oint_{\mathbf{l}} \mathbf{u} \cdot \mathrm{d}\mathbf{l} = \int_{\mathbf{S}} (\nabla \times \mathbf{u}) \cdot \mathrm{d}\mathbf{S} = \int_{\mathbf{S}} \omega \cdot \mathrm{d}\mathbf{S}. \tag{2}$$

In the above, $\mathbf{u}(x, y, z)$ represents the velocity field in a domain of interest Ω with boundary $\partial\Omega$. If the VG is included for separation control, it is also important to accurately represent its effect on the boundary-layer shape factor, H. The shape factor gives an indication of the boundary layer's ability to withstand adverse pressure gradients (and hence its susceptibility to flow separation). This integral quantity is defined as the ratio between the boundary-layer displacement thickness δ^* and momentum thickness θ, which for incompressible flow is given by

$$H = \frac{\delta^*}{\theta} = \frac{\int_0^\delta \left(1 - \frac{\mathbf{u}}{\mathbf{u}_\infty}\right) \mathrm{d}z}{\int_0^\delta \frac{\mathbf{u}}{\mathbf{u}_\infty}\left(1 - \frac{\mathbf{u}}{\mathbf{u}_\infty}\right) \mathrm{d}z}, \tag{3}$$

where δ represents the boundary-layer thickness and z is the wall-normal direction.

The above measures are a function of the velocity field only. This implies that a source term which provides an optimal match to the velocity field would be sufficient to yield the highest achievable accuracy with respect to the quantities of interest. Goal-oriented optimization using an objective function that minimizes the l^2-norm of the deviation between the velocity field and a high-fidelity reference solution $\tilde{\mathbf{u}}$,

$$J(\mathbf{u}) = \int_\Omega |\mathbf{u} - \tilde{\mathbf{u}}|^2 \, \mathrm{d}\Omega, \tag{4}$$

is therefore expected to be able to yield an optimal source term for representing the effect of a VG on the local flow field. The corresponding source term $\mathbf{f}^*$ can be calculated by solving the constrained optimization problem

$$\mathbf{f}^* = \arg\min_{\mathbf{f}} J(\mathbf{u}) \qquad \text{subject to} \qquad \mathbf{R}(\mathbf{u}, p, \mathbf{f}) = 0 \qquad \text{on} \quad \Omega, \tag{5}$$

with $\mathbf{R}(\mathbf{u}, p, \mathbf{f})$ representing the state equations and boundary conditions to be satisfied by the flow in the domain Ω. Here, $\mathbf{R}$ is defined by the incompressible Reynolds Averaged Navier–Stokes (RANS) equations,

$$\mathbf{R}_\mathbf{u} = (\mathbf{u} \cdot \nabla)\mathbf{u} + \nabla p - \nabla \cdot (2\nu D(\mathbf{u})) + \mathbf{f} = 0 \tag{6}$$

$$R_p = \nabla \cdot \mathbf{u} = 0, \tag{7}$$

where $\mathbf{R} = (\mathbf{R}_\mathbf{u}, R_p)^T$, ν denotes the kinematic viscosity (comprising both the molecular and turbulent viscosity) and $D(\mathbf{u}) = \frac{1}{2}(\nabla\mathbf{u} + (\nabla\mathbf{u})^T)$ is the strain tensor. The momentum source $\mathbf{f}$ is defined as

$$\mathbf{f} = C\,\mathbf{f}^0, \tag{8}$$

where $C = \mathrm{diag}(\mathbf{c})$ is a coefficient matrix and $\mathbf{f}_0$ an initial (uniform) forcing which is nonzero in Ω_{VG}, a subdomain enclosing the VG, so that

$$\mathbf{f}^0 = \begin{cases} \mathbf{F}^0/V_{tot} & \text{in } \Omega_{VG} \\ 0 & \text{in } \Omega \setminus \Omega_{VG} \end{cases}. \tag{9}$$

In (9), V_{tot} denotes the volume of Ω_{VG} and $\mathbf{F}^0$ is an initial estimate for the total forcing applied in Ω_{VG}. Optimization of the source-term distribution is achieved by varying the vector of control variables $\mathbf{c}$. This approach is chosen over the direct optimization of $\mathbf{f}$ in order to prevent problems due to poor scaling of the system.

2.2. Derivation of the continuous adjoint system

To solve the constrained optimization problem, Eq. (5) is reformulated as an unconstrained optimization problem using the Lagrange-multiplier method. Using the control variable $\mathbf{c}$ instead of $\mathbf{f}$, we have

$$\mathbf{c}^* = \arg\min_{\mathbf{c}} \mathcal{L}(\mathbf{u}, p, \mathbf{c}, \mathbf{v}, q), \tag{10}$$

with the Lagrange functional

$$\mathcal{L}(\mathbf{u}, p, \mathbf{c}, \mathbf{v}, q) = \int_\Omega |\mathbf{u} - \tilde{\mathbf{u}}|^2 \, \mathrm{d}\Omega + \int_\Omega \mathbf{v} \cdot \mathbf{R}_\mathbf{u}(\mathbf{u}, p, \mathbf{c}) \, \mathrm{d}\Omega + \int_\Omega q R_p(\mathbf{u}) \, \mathrm{d}\Omega, \tag{11}$$

where $\mathbf{v}$ and q are the Lagrange multipliers, often denoted as the adjoint velocity and adjoint pressure respectively. By rewriting the

constrained problem as an unconstrained problem the dimensionality of the system has increased, because we now have the adjoint variables $\lambda = (\mathbf{v}, q)$ as additional unknowns. Requiring the first-order variations of the Lagrange functional with respect to the state variables $\phi = (\mathbf{u}, p)$, the control variable $\mathbf{c}$ and the adjoint variables λ to equal zero, yields the optimality conditions

$$\delta_\phi \mathcal{L} = \nabla_\phi \mathcal{L}\, \delta\phi = 0, \tag{12}$$

$$\delta_\mathbf{c} \mathcal{L} = \nabla_\mathbf{c} \mathcal{L}\, \delta\mathbf{c} = 0, \tag{13}$$

$$\delta_\lambda \mathcal{L} = \nabla_\lambda \mathcal{L}\, \delta\lambda = 0. \tag{14}$$

These hold at the extrema of the function $\mathcal{L}$ for arbitrary variations $\delta\phi$, $\delta\mathbf{c}$ and $\delta\lambda$.

Due to linearity of $\mathcal{L}$ in λ, the last optimality condition (14) reduces to the original constraint imposed on the objective function, requiring that the state variables satisfy the state equations $\mathbf{R}(\phi) = 0$.

The first optimality condition (12), on the other hand, is more complex to solve for. Upon substitution of (11) and using

$$\delta_\phi \mathcal{L} = \delta_\mathbf{u} \mathcal{L} + \delta_p \mathcal{L} = \nabla_\mathbf{u} \mathcal{L}\, \delta\mathbf{u} + \nabla_p \mathcal{L}\, \delta p, \tag{15}$$

(12) becomes

$$\delta_\phi \mathcal{L} = \nabla_\mathbf{u} J\, \delta\mathbf{u} + \int_\Omega \mathbf{v} \cdot \nabla_\mathbf{u} \mathbf{R}_\mathbf{u}\, \delta\mathbf{u}\, \mathrm{d}\Omega + \int_\Omega \mathbf{v} \cdot \nabla_p \mathbf{R}_\mathbf{u}\, \delta p\, \mathrm{d}\Omega + \int_\Omega q\, \nabla_\mathbf{u} \mathbf{R}_p\, \delta\mathbf{u}\, \mathrm{d}\Omega. \tag{16}$$

Here the directional derivatives can be evaluated by assuming Fréchet differentiability and by making use of the Gâteau derivative. This approach is similar to the one used in [15] and, for the assumption of frozen turbulence, yields the adjoint momentum and continuity equations

$$\nabla\mathbf{v} \cdot \mathbf{u} + (\mathbf{u} \cdot \nabla)\mathbf{v} + 2\nu\nabla \cdot D(\mathbf{v}) - 2(\mathbf{u} - \tilde{\mathbf{u}}) = \nabla q \tag{17}$$

$$\nabla \cdot \mathbf{v} = 0, \tag{18}$$

with boundary conditions derived from

$$\int_{\partial\Omega} [\mathbf{n}(\mathbf{v} \cdot \mathbf{u}) + \mathbf{v}(\mathbf{u} \cdot \mathbf{n}) + 2\nu\mathbf{n} \cdot D(\mathbf{v}) - q\mathbf{n}] \cdot \delta\mathbf{u}\, \mathrm{d}S - \int_{\partial\Omega} 2\nu\mathbf{n} \cdot D(\delta\mathbf{u}) \cdot \mathbf{v}\, \mathrm{d}S = 0 \tag{19}$$

$$\int_{\partial\Omega} (\mathbf{v} \cdot \mathbf{n}) \delta p\, \mathrm{d}S = 0, \tag{20}$$

which should hold for arbitrary variations $\delta\mathbf{u}$ and δp.

Finally, the variation of the Lagrangian with respect to the control variable is considered. Since (13) should be satisfied for arbitrary variations $\delta\mathbf{c}$, this reduces to an expression that allows for the direct calculation of the sensitivity of $\mathcal{L}$ with respect to $\mathbf{c}$, and given (14) therefore also of J. The sensitivity of the cost function w.r.t. the source coefficients $\mathbf{c}_i$ in a cell i thus becomes

$$\nabla_{\mathbf{c}_i} \mathcal{L} = \nabla_{\mathbf{c}_i} J = \int_\Omega \mathbf{v} \cdot \nabla_{\mathbf{c}_i} \mathbf{R}_\mathbf{u}(\mathbf{u}, p, \mathbf{c})\, \mathrm{d}\Omega = \mathrm{diag}(\mathbf{v}_i)\, \mathbf{f}_i^0 V_i, \tag{21}$$

with V_i the volume of cell i.

Despite the cost of having to solve the additional system of adjoint equations, the advantage of this methodology is that it allows for the direct calculation of the sensitivity of the objective function with respect to the control variable. As (21) is inexpensive to calculate, this implies that with only the computational cost equivalent to two state-equation solves one is able to obtain the necessary sensitivity information to use a gradient optimization algorithm to calculate $\mathbf{c}^*$, and therefore the optimal source term $\mathbf{f}^*$.

Note that the presented derivation makes use of Taylor's hypothesis (the frozen-turbulence assumption), which assumes that derivatives of the turbulent quantities (the eddy viscosity) with respect to the state variables are negligible. As this implies an incomplete derivative in (12), the obtained sensitivities are no longer exact. However, this comes at the advantage of not having to solve additional equations for the adjoint turbulence variables. Despite the possibility of large sensitivity errors [16], in general the assumption is valid for cases where the integral scales are sufficiently large compared to the smaller scales [17], hence cases with a low turbulence intensity. For example, in [18] it is shown (for a discrete adjoint approach) that the assumption of constant eddy viscosity yields excellent results for a high-lift airfoil case. For the sake of computational expediency, in the current work we therefore assume the frozen-turbulence assumption to have little impact on the optimization process. As will be shown in Section 5, the accuracy of the obtained results indicates that this assumption is indeed valid for our purpose.

2.3. Gradient optimization approach

The optimality conditions defined by (12), (13) and (14) must all be satisfied at an optimum. In [19] a one-shot approach is proposed, solving for all three conditions simultaneously using a reduced SQP-type method. Despite some promising results, the most straightforward and widely used approach consists of first solving the system of state and adjoint equations, and using the sensitivity of the cost function in an outer gradient-optimization loop [15,20,21]. In [21] several limited-memory quasi-Newton line search optimization methods are tested in the context of DNS-based optimal control of turbulent flows. It was found that the L-BFGS approach performed best among the tested methods, requiring the smallest overall computational cost, with the damped L-BFGS method being most efficient. The latter is attributed to its small numerical overhead per iteration, compensating for the larger number of required iterations due to its less accurate Hessian approximation, compared with standard L-BFGS.

In this work, however, we prefer the use of a trust-region (TR) optimization method instead of a line-search method. As the majority of the computational cost is attributed to the evaluation of the cost function, requiring the solution of the state and adjoint systems, a low number of iterations is considered more important than the overhead of the iterative scheme per iteration. Furthermore, TR methods are generally more robust when dealing with nearly singular systems [22]. We therefore make use of a TR inexact Newton optimization scheme, in combination with a modified conjugate-gradient (CG) algorithm due to Steihaug [23] and approximating the Hessian matrix with the L-BFGS method. The latter is a low-memory variation to the Broyden–Fletcher–Goldfarb–Shanno updating scheme, reconstructing the Hessian every iteration using only the gradient information of the most recent iterations. The implementation of our optimization method is similar to that in [22]. An overview of the steps involved is given in Fig. 1b.

It should be noted that this TR optimization approach is only able to find a local optimum. Moreover, by the choices we make for the shape of the source term, both through the selection of Ω_{VG}, where $\mathbf{f}$ is to be applied and optimized, and through our choice for $\mathbf{f}_0$ as (8), we impose a restriction on the achievable accuracy. Hence, it might be possible that a source term with a different initial shape than studied in this work is more effective in reproducing the reference flow field. For example, in theory a source term that is defined in every cell of the domain would be more effective in minimizing J. However, such a source term would be impractical for the application of VG models.

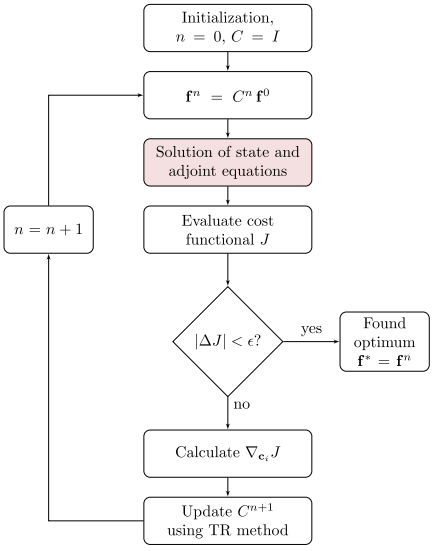

(a) Overview of the source-term optimization implementation. The computationally most expensive part consists of the state and adjoint system solves, indicated in red.

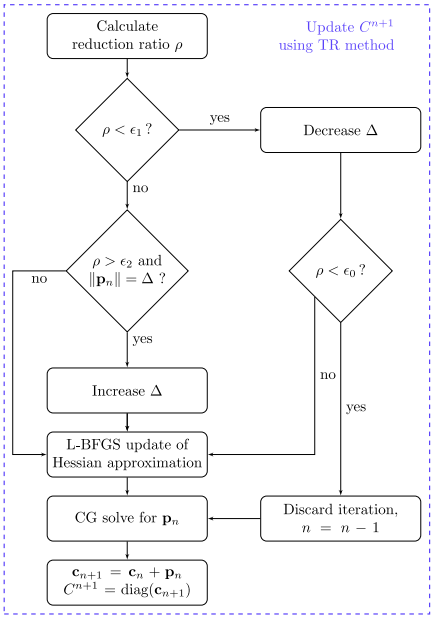

(b) Steps involved in the TR Newton CG optimization approach to update the control vector $\mathbf{c}$. The reduction ratio ρ is defined as the ratio between the achieved and predicted reduction in J, and is used to determine whether the trust region size Δ should be reduced or increased, where $0 < \epsilon_0 < \epsilon_1 < \epsilon_2 < 1$.

Fig. 1. Schematic overview of the proposed source-term optimization approach.

2.4. Implementation details

The described methodology has been implemented in the open-source CFD package OpenFOAM, which is a segregated finite-volume code able to solve both compressible and incompressible flows using either structured or unstructured grids. A basic shape-optimization algorithm is already contained in the package [15], which served as the starting point for our source-term optimization method. The steady incompressible RANS equations and their continuous-adjoint counterpart are solved in a coupled fashion by making use of the SIMPLE algorithm. Once a steady-state solution is obtained, the cost functional is evaluated and its sensitivity with respect to the control variable is calculated from (21). The source term is then updated using the trust-region approach, described in Section 2.3, until a local optimum is found. This process is visualized in Fig. 1a and b.

During the initialization step, Ω_{VG} is defined by selecting where the source term is to be applied. This roughly corresponds to the location of the VG (see Section 3.1). In the selected cells an initial forcing per unit volume $\mathbf{f}_{0_i}$ is defined, according to Eq. 9, based on a user-defined input vector $\mathbf{F}_0$ (for each VG considered) which represents an estimate for the total forcing the presence of the VG would impose on the flow. This estimate does not need to be accurate, however, it is important that all components are non-zero. Note that the control variables $\mathbf{c}_i$ are vectors defined for the cells contained in Ω_{VG} only, yielding a total of $3N_{VG}$ controls to be optimized, with N_{VG} the number of cells in the VG domain Ω_{VG}.

3. Description of study

3.1. Approach

It is assumed that a body-fitted mesh (BFM) simulation solving the same governing equations yields the highest accuracy one can aim to achieve with a source-term model simulation. In this work we use a RANS approach for the BFM simulation, however, the use of a large-eddy simulation (LES) would also be possible. As visualized in [14], this choice implies that errors introduced by the RANS approach are outside the scope of the current study, and only model errors (due to the replacement of the geometry by a source term) and discretization errors are taken into account. Hence, when considering the objective function (4), the high-fidelity reference solution $\tilde{\mathbf{u}}$ consists of the projection of the corresponding BFM solution onto the source-term model mesh. Furthermore, the surface force acting on the VG surface as obtained from the BFM simulation is used as $\mathbf{F}_0$ in (9) to define the initial source-term distribution from which to start the optimization.

The flow field obtained when using an optimized source term is compared to (i) the BFM result, and (ii) the corresponding result obtained using the jBAY model. The jBAY model [13] is currently the most widely used source-term model when performing CFD simulations involving VGs. It is an adaptation of the original BAY model proposed by Bender et al. [11], which represents the effect of a VG on the flow by the addition of a lateral body force,

$$\mathbf{f}_i^{BAY} = cA\frac{V_i}{V_{tot}}\rho(\mathbf{u}_i \cdot \mathbf{n})(\mathbf{u}_i \times \mathbf{b})\left(\frac{\mathbf{u}_i}{|\mathbf{u}_i|} \cdot \mathbf{t}\right), \tag{22}$$

to the momentum equation in those cells that correspond to the VG location. In the above, $\mathbf{t}$, $\mathbf{n}$ and $\mathbf{b}$ are unit vectors representing respectively the tangential, normal and spanwise VG directions, A is the VG surface area and c a constant which to some extent can be used for calibration. The addition of Jirasek [13], resulting in the jBAY model, consist of an alternative cell-selection approach in combination with interpolation and redistribution of the source term in order to reduce mesh dependency of the model.

Optimization of the source term was initially performed for Ω_{VG} being a rectangular domain enclosing the VG, see Fig. 2a. Then, in order to facilitate the comparison between our optimized source

(a) Cell selection A: rectangular domain enclosing the VG. (b) Cell selection B: cells aligned with the VG.

Fig. 2. Visualization of the two approached used to select the cells where the source term is applied.

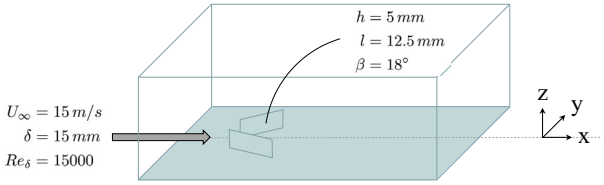

Fig. 3. Overview of the configuration used to test the proposed source-term optimization approach.

Table 1
Overview of the used numerical meshes for the body-fitted mesh (BFM) and the source-term (M0, M1 & M2) simulations.

	Single VG		VG Pair	
	N	N_c	N	N_c
BFM	1.7×10^6	96	4.9×10^6	176
M0	–	–	0.1×10^6	15
M1	0.1×10^6	25	0.4×10^6	30
M2	0.4×10^6	50	1.6×10^6	60

term and the jBAY model, also the same cells used by the jBAY model where used to define Ω_{VG}. These correspond to the physical location of the VG, as shown in Fig. 2b. These two Ω_{VG} selection approaches will be referred to as methods A and B, and the optimal source terms calculated in these regions as OSTA and OSTB, respectively. Considering both approaches allows to study the effect of the selected cells on both the source-term distribution pattern and the achievable accuracy (i.e. the reduction in J and the shape-factor error ϵ_H).

For all simulations presented in the remainder of this work, structured hexahedral grids are used with second-order upwind descretization schemes for the convective terms. Closure of the RANS equations is provided by Menter's $k-\omega$ SST turbulence model, with the near wall spacing of the meshes being sufficiently dense ($y^+ < 1$) for the viscous sublayer to be resolved. Note that the same numerical settings are used for both the state and adjoint equations.

3.2. Test cases

Our approach is demonstrated by application to turbulent wall-bounded flows over a flat plate with VGs, which mainly affect the inner part of the boundary layer. Initially the implementation is tested for one of the experimental set-ups as studied by Yao et al. [24], comprising a single submerged VG with $h/\delta = 1/5$ and an incidence angle of $\beta = 16^\circ$ w.r.t. the incoming flow (for which $U_\infty = 34$ m/s).

Afterward the experimental setup of Baldacchino et al. [25] is used for further analysis. This configuration consists of a flat plate with submerged ($h/\delta = 1/3$) rectangular counter-rotating common-down VGs, and is also used for the numerical investigation presented in [14], including BFM, BAY and jBAY model simulations. An overview of this configuration including relevant parameters is included in Fig. 3. In this work, numerical settings similar to those in [14] are used. This means that only one VG pair is included in the simulations, with the effect of neighboring vortices accounted for by making use of symmetry boundary conditions. The boundary conditions for the other sides (i.e. the bottom plate and the inlet, outlet and top of the domain) are discussed in Section 3.3.

For the reference BFM simulation of the VG pair a mesh similar to that in [14] is used, where the mesh independence of the corresponding solution was evaluated, yielding an avarage discretization error w.r.t. the downstream shape factor H of 0.3%. For the current study the numerical domain is slightly reduced in both streamwise and wall normal direction in order to limit the computational cost. Using a similar approach, also a body-fitted mesh is constructed for the case with an isolated VG. For this case the average discretization error for H was found to be 0.3% as well, thus indicating a mesh-independent reference solution.

For the jBAY and optimized $\mathbf{f}$ simulations an empty flat plate is considered, for which uniform meshes of different resolutions were created. The coarsest meshes consisted of 25 and 16 cells in crossflow direction for the simulated single VG and VG pair respectively, corresponding to a resolution of only $\Delta = 0.7h$ and $\Delta = 0.4h$, in both streamwise and crossflow direction. Medium (M1) and fine (M2) meshes were subsequently created by factor 2 and 4 refinements, in both the x- and y-directions. In the wall normal (z-) direction, the same mesh spacing was used as for the BFM simulation for all cases, such that even on the coarsest mesh the boundary layer is sufficiently resolved. The mesh details are summarized in Table 1, and snapshots are included in Fig. 4.

3.3. (Adjoint) boundary conditions

Whereas determination of the boundary conditions for the primal (state) equations is rather straightforward, the boundary conditions for the adjoint velocity and adjoint pressure ($\mathbf{v}$ and q) need to be calculated from the integral equations (19,20) by substitution of the corresponding primal boundary conditions. Below, this is done for the different types of boundaries encountered in our test problems.

Walls and inlet. Both the wall surfaces and the inlet boundary (on the left side of the domain for $x = 0$) are characterized by a fixed velocity and a zero gradient condition for the pressure, hence

$$\mathbf{u} = \text{const} \qquad \text{and} \qquad \nabla p = 0. \tag{23}$$

From (20), which should hold for arbitrary δp, it immediately follows that along these boundaries we have

$$\mathbf{v} \cdot \mathbf{n} = 0. \tag{24}$$

Moreover, the condition on $\mathbf{u}$ implies $\delta\mathbf{u} = 0$ such that (19) reduces to

$$\int_\Gamma 2\nu\mathbf{n} \cdot D(\delta\mathbf{u}) \cdot \mathbf{v}\,\mathrm{d}S = \int_\Gamma \nu\mathbf{n} \cdot \left[\nabla\delta\mathbf{u} + (\nabla\delta\mathbf{u})^T\right] \cdot \mathbf{v}_t\,\mathrm{d}S = 0. \tag{25}$$

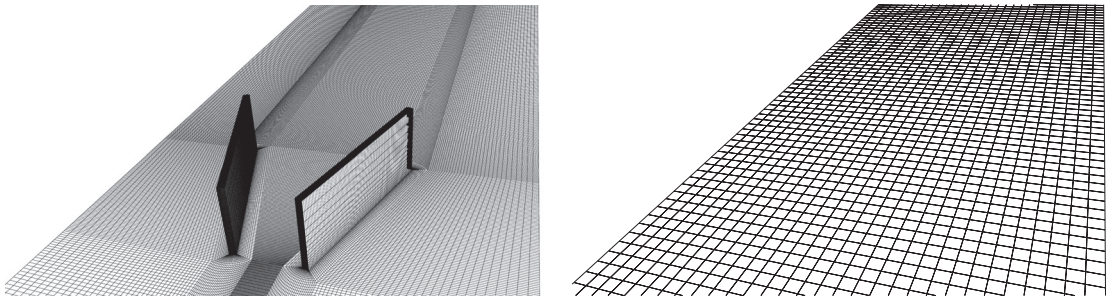

(a) Body-fitted mesh. (b) Uniform mesh for the source term simulations (M1).

Fig. 4. Snapshot of the used numerical meshes for the VG pair case.

The above is always satisfied by requiring the tangential adjoint-velocity component to be zero as well. The boundary integral equations do not yield a condition for the adjoint pressure. Similar to [15] we therefore exploit the similarity between the primal and adjoint equations and use

$$\mathbf{v} = 0 \qquad \text{and} \qquad \nabla q = 0 \tag{26}$$

as boundary conditions for the adjoint variables along the walls and inlet.

Outlet. At the outlet of the domains we require the flow to be parallel to the surface, and we prescribe a constant value for the pressure. The primal boundary conditions for the outlet are therefore

$$\mathbf{n} \cdot \nabla \mathbf{u} = 0 \qquad \text{and} \qquad p = \text{const.} \tag{27}$$

The latter implies that $\delta p = 0$ such that (20) is automatically satisfied. Furthermore, it is shown in [15] that (19) is equivalent to

$$\int_\Gamma [\mathbf{n}(\mathbf{v}\cdot\mathbf{u}) + \mathbf{v}(\mathbf{u}\cdot\mathbf{n}) + \nu(\mathbf{n}\cdot\nabla)\mathbf{v} - q\mathbf{n}]\cdot\delta\mathbf{u}\,\mathrm{d}S - \int_\Gamma \nu(\mathbf{n}\cdot\nabla)\delta\mathbf{u}\cdot\mathbf{v}\,\mathrm{d}S = 0, \tag{28}$$

where the last integral cancels because $\mathbf{u}+\delta\mathbf{u}$ should satisfy the boundary condition for $\mathbf{u}$ and therefore $\mathbf{n}\cdot\nabla\delta\mathbf{u} = 0$. Decomposition of the first integral of (28) into its normal and tangential components then yields the conditions for the adjoint pressure and velocity at the outlet,

$$q = \mathbf{v}\cdot\mathbf{u} + v_n u_n + \nu\mathbf{n}\cdot\nabla v_n \tag{29}$$

$$0 = u_n\mathbf{v}_t + \nu\mathbf{n}\cdot\nabla\mathbf{v}_t. \tag{30}$$

Top. Along the boundary on the top of the domains zero-gradient requirements hold for the state variables, hence

$$\mathbf{n}\cdot\nabla\mathbf{u} = 0 \qquad \text{and} \qquad \nabla p = 0. \tag{31}$$

Similar to the wall and inlet boundaries, from Eq. (20) it therefore follows that

$$\mathbf{v}_n = 0, \tag{32}$$

whereas similar to the outlet boundary, (19) implies that the adjoint pressure and tangential velocity should satisfy (29) and (30) respectively.

Sides. Finally, the side boundaries parallel to the flow direction act as symmetry planes, thereby simulating the effect of neighboring VGs in order to create a VG array. For the single VG case, the width of the domain is chosen large enough such as to eliminate the effect of the neighboring vortices.

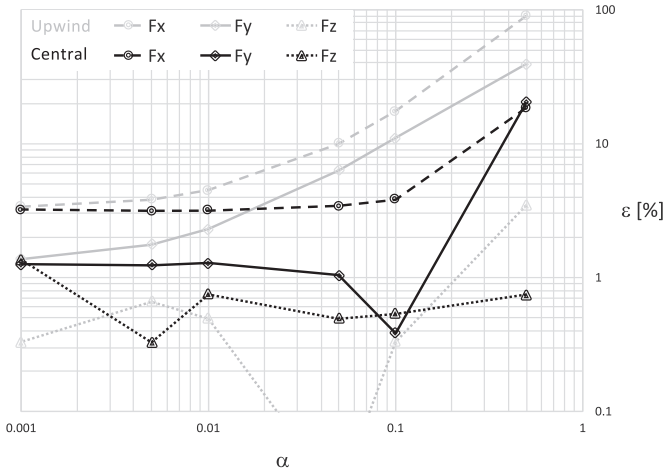

Fig. 5. Relative difference between the adjoint-based and finite-difference approximated gradients related to the total source-term forcing in x-, y- and z-direction.

4. Validation of the adjoint-based gradient

The adjoint-based gradient of the objective function with respect to the source-term coefficients $\mathbf{c}_i$, defined by (21), is validated against finite-difference approximations for the single VG test case. As the total number of controls is typically large ($3N_{VG}$), and finite-difference approximations require at least one function evaluation per control change, it is chosen to study the sensitivity to overall changes in the x-, y- and z-component, rather than considering the sensitivity to changes in separate cells. Therefore simulations have been performed starting from a uniform source-term distribution in Ω_{VG}, and subsequently imposing a perturbation that is equal in all cells.

When making use of finite-difference discretizations, the sensitivity of J to changes in the x-component of $\mathbf{c}$ can thus be approximated as

$$\nabla_{c_x} J^{FD,c} = \frac{J(\mathbf{u}(c_x + \alpha c_x)) - J(\mathbf{u}(c_x - \alpha c_x))}{2\alpha} \qquad \text{and}$$
$$\nabla_{c_x} J^{FD,u} = \frac{J(\mathbf{u}(c_x + \alpha c_x)) - J(\mathbf{u}(c_x))}{\alpha}, \tag{33}$$

for central and upwind schemes respectively, with α the step length. Equivalently, the overall adjoint-based sensitivity to a global change in the x-component of $\mathbf{c}$ equals

$$\nabla_{c_x} J^{ADJ} = \sum_{i=1}^{N_{VG}} \nabla_{c_{x_i}} J. \tag{34}$$

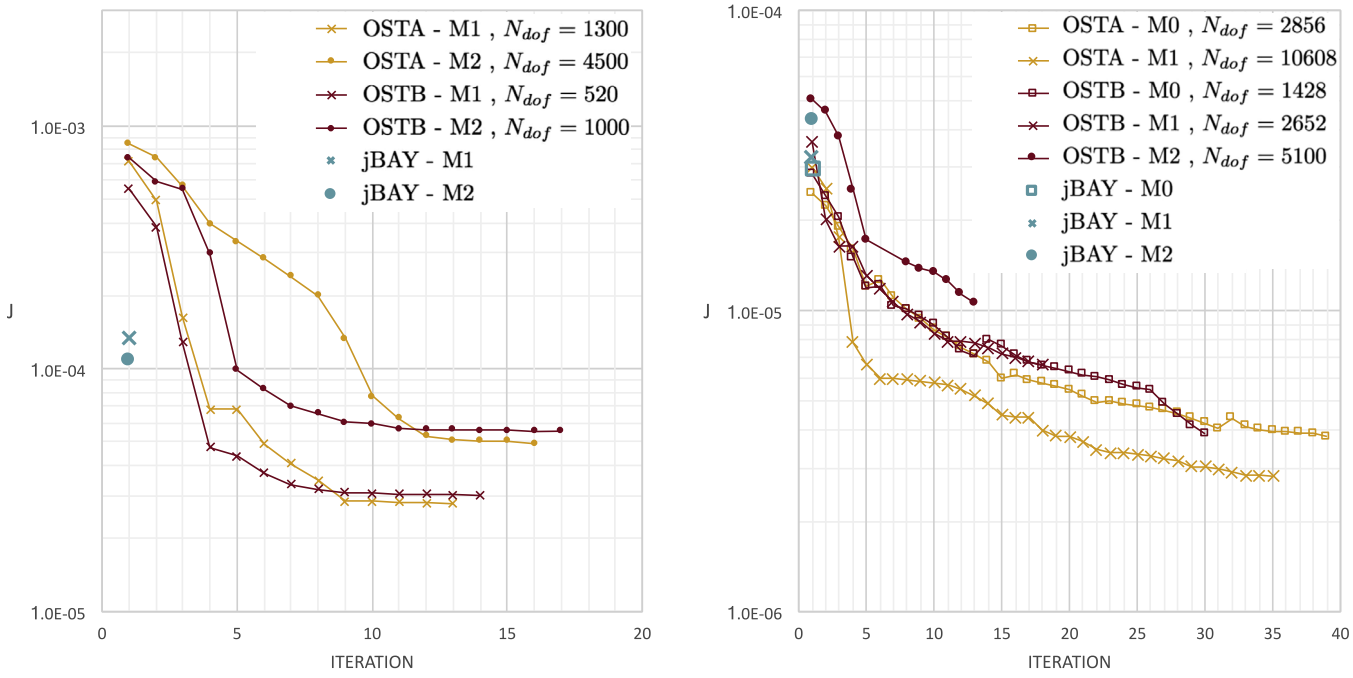

(a) Single VG (b) VG pair

Fig. 6. Convergence of the source-term optimization algorithm, with the computational cost related to 1 iteration approximately equal to the cost for 1 jBAY model solve.

In Fig. 5 the normalized difference between the adjoint-based and finite-difference sensitivities, defined as

$$\epsilon = \frac{|\nabla_{c_x} J^{FD} - \nabla_{c_x} J^{ADJ}|}{\nabla_{c_x} J^{ADJ}} \cdot 100\%, \tag{35}$$

is shown for different step lengths α. From these results it follows that the relative error converges to approximately 3%, 1% and 0.5% for c_x, c_y and c_z respectively. The remaining deviations are likely attributable to our use of the frozen-turbulence assumption. Overall, this validation indicates good reliability of the adjoint-based gradients, which are considered sufficiently accurate for the intended purpose.

Table 2
Objective-function values J for various mesh resolutions as obtained with the jBAY model and the optimized source terms. The 'IC' result corresponds to the initial condition (boundary layer without VGs), before starting the optimization with J evaluated on $\Omega \backslash \Omega_{VG}$ and Ω_{VG} determined according to method B.

		IC	jBAY	OSTA	OSTB
Single VG	M1	2.88×10^{-3}	1.34×10^{-4}	2.78×10^{-5}	3.01×10^{-5}
	M2	2.93×10^{-3}	1.09×10^{-4}	4.93×10^{-5}	5.54×10^{-5}
VG Pair	M0	2.77×10^{-4}	2.98×10^{-5}	3.84×10^{-6}	3.89×10^{-6}
	M1	2.78×10^{-4}	3.21×10^{-5}	2.63×10^{-6}	6.68×10^{-6}
	M2	2.88×10^{-4}	4.35×10^{-5}	–	1.12×10^{-5}

5. Accuracy improvement when using an optimized source term

In this section the results obtained with an optimized source term are presented and discussed. These are optimized with respect to $\tilde{\mathbf{u}}$, the projection of the BFM flow field onto the low-resolution meshes used for the source-term simulations, where $\tilde{\mathbf{u}}$ differs only slightly from the original high-resolution BFM result. The single VG case is used for the initial testing of the optimization framework, while the majority of the analysis is focused on the more complex VG pair case, involving the interaction between neighboring vortices. In the remainder, OSTA refers to the result obtained using an optimized source term with Ω_{VG} defined by selection method A, whereas for OSTB selection method B used.

For both flat-plate test cases considered, a source term that significantly decreases the flow deviation with respect to the projected BFM solution is obtained for both methods OSTA and OSTB. This is illustrated by the objective-function results presented in Table 2, which contains the $J(\mathbf{u})$ values for (i) the initial condition (IC) consisting of an undisturbed boundary layer, (ii) the resulting flow field when simulating the presence of VGs using the jBAY model, (iii) the result when the source term is optimized in a rectangular area enclosing the VG (OSTA), and (iv) the flow field obtained with a source term that is optimized in the cells corresponding to the VG location (OSTB). Whereas the jBAY model decreases the flow deviation by one order of magnitude compared to the undisturbed boundary layer, the use of a goal-oriented optimized source term is able to decrease the flow deviation by almost another order of magnitude. A much better correspondence with the BFM results is thus obtained with the optimized source terms than with the jBAY model, for all cases considered.

Furthermore, Table 2 shows that for cell-selection method B (so both the jBAY and OSTB results) the lowest value for the objective function is obtained on the coarsest mesh and that J increases with mesh refinement. This, however, does not mean that the obtained flow field becomes a worse representation of the VG-induced flow upon mesh refinement (as can be seen in Figs. 7 and 11). Rather, these relatively high J values on meshes M1 and M2 are attributed to the reducing size of Ω_{VG}. Since $J(\mathbf{u})$ is evaluated on the entire domain except Ω_{VG}, for selection method B mesh refinement implies that the velocity deviation is measured in a region closer to the VG surface, where in the BFM results a boundary layer is present. This causes an increase in the overall velocity deviation, as in this region the largest differences with respect to the BFM result are found, even though the representation of the flow downstream has still improved (Figs. 7 and 11). This increasing J phenomenon is

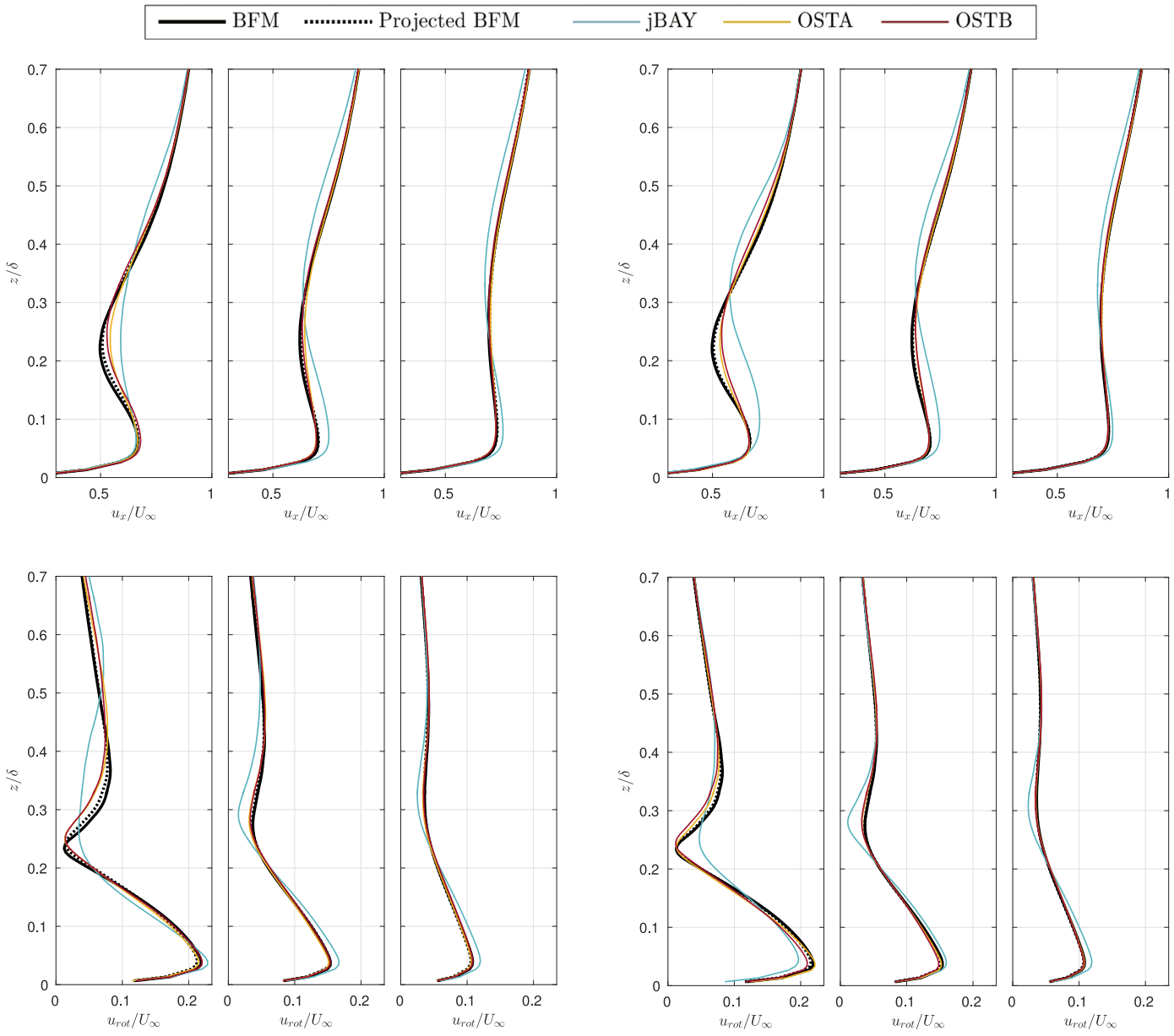

(a) Mesh M0 (b) Mesh M1

Fig. 7. Streamwise (u_x) and rotational (u_{rot}) velocity profiles for $y = y_{TE}$ at (from left to right) $\Delta x/h = 5$, $\Delta x/h = 10$ and $\Delta x/h = 15$, VG pair case.

not observed for method A, as in that case Ω_{VG} remains constant upon mesh refinement.

The cost related to the source-term optimization is minimal, despite the large number of degrees of freedom considered (ranging from $N_{dof} = 520$ for the single VG OSTB result on mesh M1 to $N_{dof} = 10680$ for the VG pair OSTA result on mesh M1). The convergence results in Fig. 6 show that the main drop in objective function is obtained within the first 10 iterations, independent of the number of degrees of freedom. It is found that the average computational cost per iteration is approximately equal to the cost related to one flow simulation with the jBAY model. This suggests that, independent of the mesh size and the number of cells over which the source term is distributed, in general a largely improved source term can be obtained while keeping the computational cost limited to the cost equivalent to 10 jBAY simulations.

Our results clearly show that a low mesh resolution does not prohibit the reproduction of a highly accuracy VG-induced flow field. For the most complex case considered, involving the interaction of two vortices emerging from a VG pair, even on the coarse mesh M0 Fig. 7 shows a much improved agreement in velocity profile, both for the dominant streamwise velocity component u_x, and the secondary rotational velocities $u_{rot} = \sqrt{u_y^2 + u_z^2}$. The low objective-function values therefore indeed indicate the creation of a physically meaningful flow field. This is confirmed by the improved modeling of the total flow circulation and the created vortex core, shown in Figs. 9 and 8 respectively. By obtaining a higher accuracy for the circulation and the vortex-core size and location, the optimized source term approach ensures that the interaction of the vortices with the wall and their neighbors can be predicted with a high reliability.

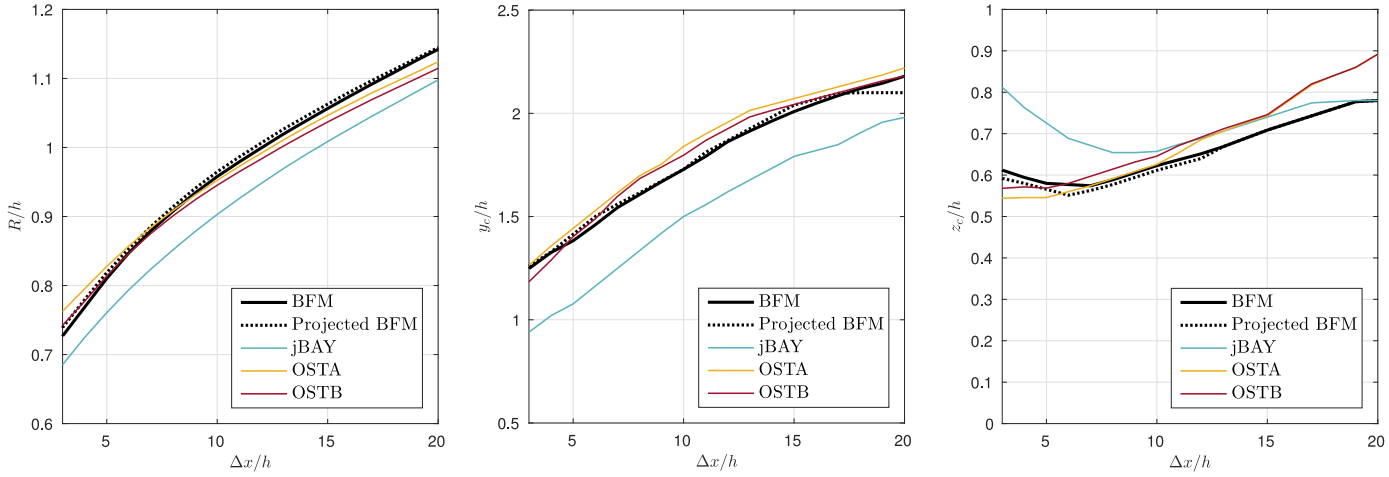

(a) Radius of an equivalent circular vortex. (b) Center location in y-direction. (c) Center location in z-direction.

Fig. 8. Vortex-core characteristics for the VG pair case, mesh M1.

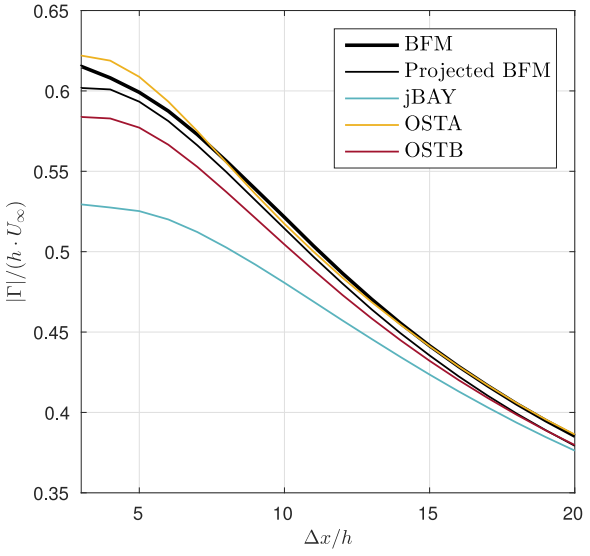

Fig. 9. Total circulation due to 1 VG of the VG pair case, calculated by considering the vortex region for which the streamwise vorticity $\omega_x \leq 0.1\omega_{x,\,max}$.

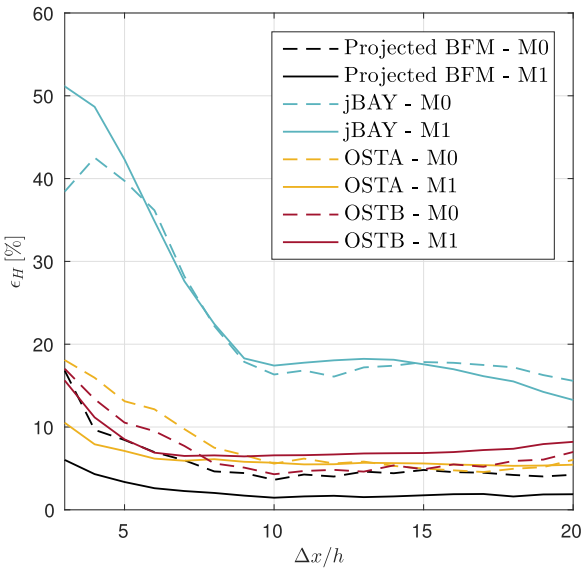

Fig. 10. Shape-factor error for the VG pair case, computed as the mean deviation from the BFM result and normalized with the deviation in H with respect to an undisturbed boundary layer.

It follows from Fig. 11 that on all considered meshes the optimized source terms therefore indeed achieve the primary goal of reducing the shape-factor error. A visual improvement of the shape-factor profiles is observed, with the extrema and inflection points now being situated at the correct locations. Even for the coarsest mesh used to simulate the effect of a single VG (M1, with $\Delta \approx 0.7$ h), a source term is obtained that yields an excellent representation of the effect of the vortex-formation process on the local boundary layer.

However, it is also observed from Fig. 11 that the shape-factor extrema are not completely resolved, and this error does not decrease with downstream distance of the VG. This is probably attributable to the limited mesh resolution, as it is clear from comparison between the VG pair results on meshes M0 and M1 that the error in the peak values is smaller for the finest mesh considered. The results also show that the choice of Ω_{VG} has an influence, although the difference between the OSTA and OSTB results reduces downstream. In the following sections, the OSTA and OSTB approaches are discussed in more detail.

Overall, the shape-factor error is reduced significantly using an optimized source term when compared to the jBAY results, even on very coarse meshes. Fig. 10 shows that for the entire domain the error is at least halved. The largest reduction is found in the first 10 h behind the VG pair. This corresponds to the region with the weakest interaction between the vortex core and the turbulent length scales, and therefore the region which best represents the effect of the source term. This allows to conclude that our optimization framework is successful in calculating reliable source-term distributions to represent VG effects on a wall-bounded flow, and that the frozen-turbulence assumption has not significantly impacted the results.

6. Optimal source term using selection method A (OSTA)

OSTA is considered the most general source-term optimization approach, as Ω_{VG} can be chosen arbitrarily. In our case Ω_{VG} consists of a rectangular region enclosing the VG(s) of the test case, thereby basically being unrelated to the VG geometry. This se-

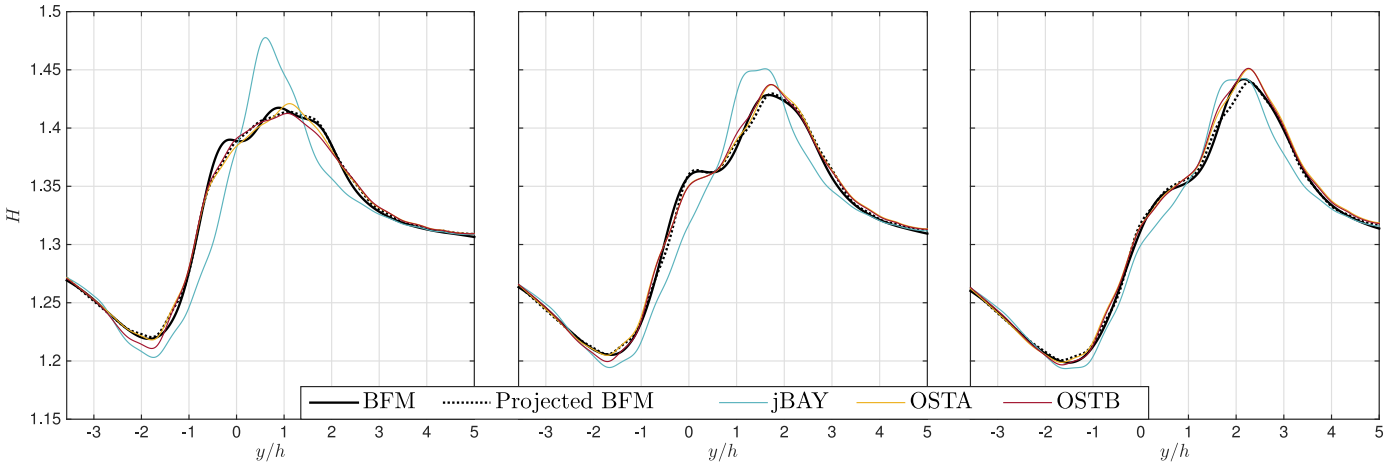

(a) Single VG, mesh M1

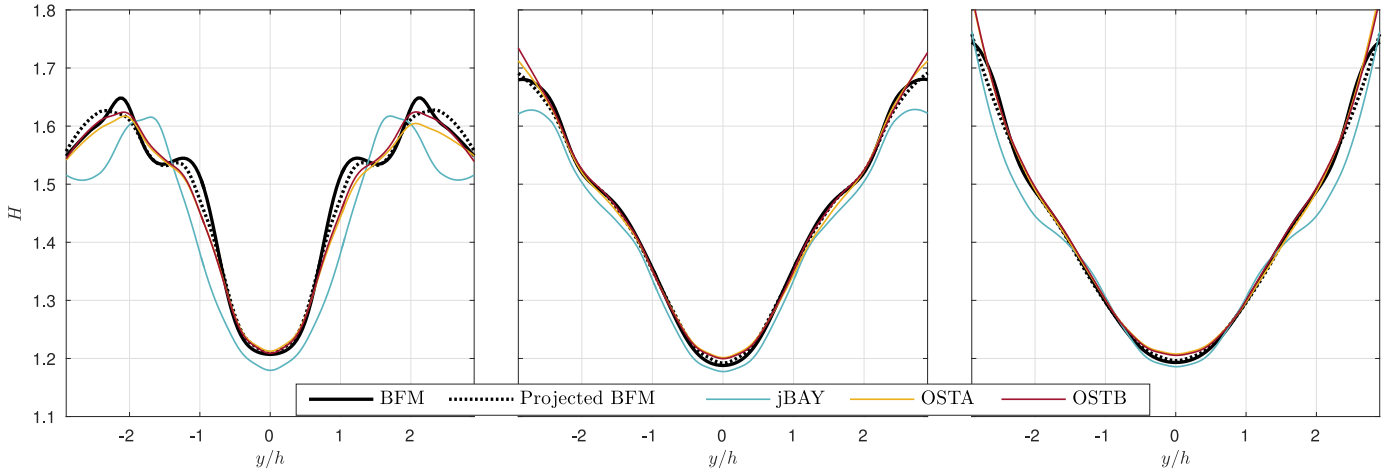

(b) VG pair, mesh M0

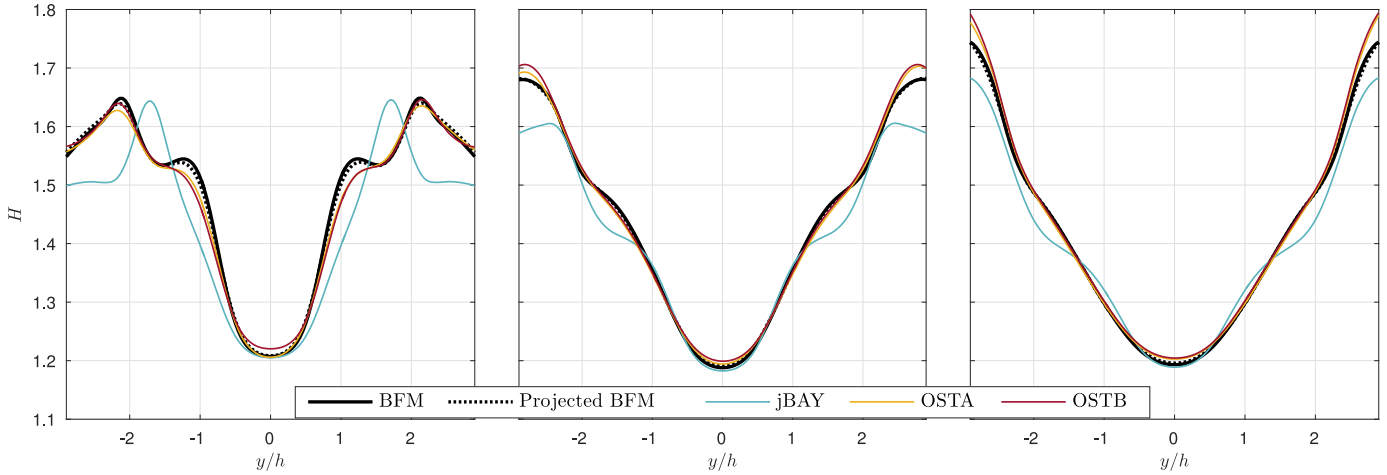

(c) VG pair, mesh M1

Fig. 11. Shape factor profiles at (left to right) $\Delta x/h = 5$, $\Delta x/h = 10$ and $\Delta x/h = 15$.

lection method allows for a smooth distribution of the resulting source term, due to its large freedom for choosing Ω_{VG} such that the source term can be distributed over a large region. This is an interesting feature, as it shows the potential for using coarse meshes.

The OSTA source term obtained for the VG pair on mesh M1 is shown in Fig. 12, for a plane parallel to the surface and located at half the VG height. As expected, it follows that the obtained source term basically aims to impose the created vortices onto to the undisturbed boundary layer. For example, the component in z-

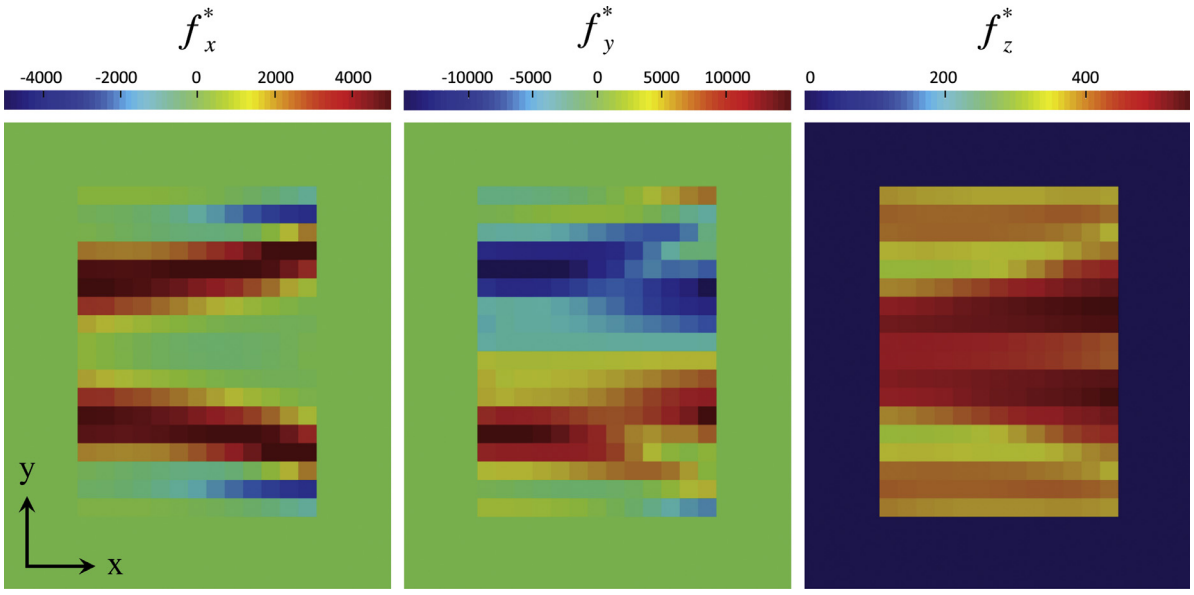

Fig. 12. Top view of the OSTA optimal source-term components (as force per unit volume) in x-, y- and z-direction, for a plane at $z = h/2$. Note that due to the sign of **f** in (6) the displayed body forces are opposite to their effect on the velocity field.

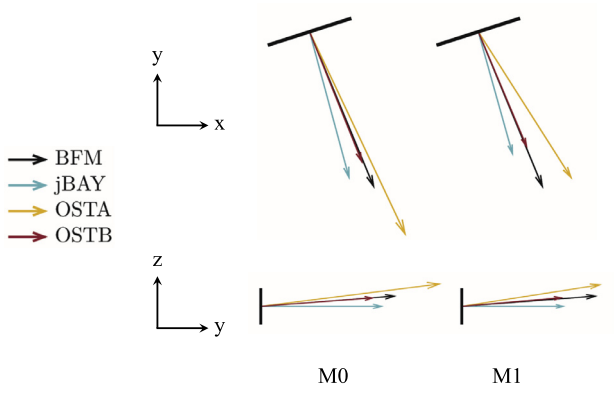

Fig. 13. Top and side view illustrating the magnitude and direction of the resultant source term forcing.

direction clearly introduces the downwash typically observed between a vortex pair, whereas the component in x-direction shows similarities with the separation region on the suction side of the VGs. Although Ω_{VG} comprises the region of vortex creation, involving the most complicated flow patterns, OSTA is observed to be successful (see Section 5), even on the coarsest mesh considered and employing a rather small Ω_{VG}.

By increasing the domain Ω_{VG}, especially in case of coarse meshes, it is expected that the accuracy of the OSTA results can be even further improved, as the numerical diffusion can be compensated in a larger part of the domain. Hence, when considering $\Omega_{VG} = \Omega$, thus adding a source term in the entire flow domain, in theory a perfect match in flow field can be obtained. From a practical viewpoint, however, this situation is undesirable. In reality, the choice for Ω_{VG} will therefore often be a trade-off between accuracy and practicality.

Note that the obtained source term seems to be in line with the rationale behind vortex-profile VG models [8,9], which typically impose a developed vortex profile downstream of the VG. The outstanding accuracy of the OSTA result, compared to these existing models, can be attributed to the case-specific vortex profile that is imposed. However, it is expected that the inclusion of the vortex-creation process is equally or even more important, as it allows for a more natural and smooth adaptation of the boundary layer.

The presented OSTA results demonstrate that, with a suitable source term, even on very coarse meshes an accurate representation of a VG-induced flow field can be obtained. Furthermore, the approach allows to assess whether mesh refinements are required in order to reach a specific simulation goal. Apart from the academic significance, this notion and the developed approach can also be of interest for industry, where typically flow simulations are required for large geometries including numerous VGs with a similar design (for example a wind-turbine blade). An OSTA approach might be used as part of a multi-fidelity modeling framework, allowing for accurate source-term simulations of these large structures with minimal mesh requirements. The construction of a BFM is rather straightforward for a single VG, and the BFM simulation computationally inexpensive. With only minimal effort it is therefore possible to calculate an optimized source term for a coarse mesh of interest. By doing this for a range of expected inflow conditions, optimal source terms can be calculated and imposed at every VG location in order to include the effect of VGs in the large-scale simulation of the overall structure. Theoretically, this way it might be possible to obtain highly-accurate flow results at a reasonable computational cost, and without the tedious task of creating a suitable mesh for the overall structure including VGs. Further research is however required in order to investigate the feasibility of such a multi-fidelity approach.

7. Optimal source term in region corresponding to VG location (OSTB)

The OSTB approach basically forms a special case of OSTA, as in this case the domain Ω_{VG} is limited to the cells corresponding to the VG location, as shown in Fig. 2b. Apart from the reduction in degrees of freedom for the optimization problem, limiting the domain to these particular cells holds the advantage of allowing investigation of the full potential behind the jBAY modeling approach, i.e. that the addition of VG surface reaction forces could result in a suitable vortex. Due to the particular shape and limited size of Ω_{VG}, the OSTB approach does not allow for the creation of a source term that imposes a (fully-developed) vortex, but rather is forced to focus on the driving force that causes the creation of

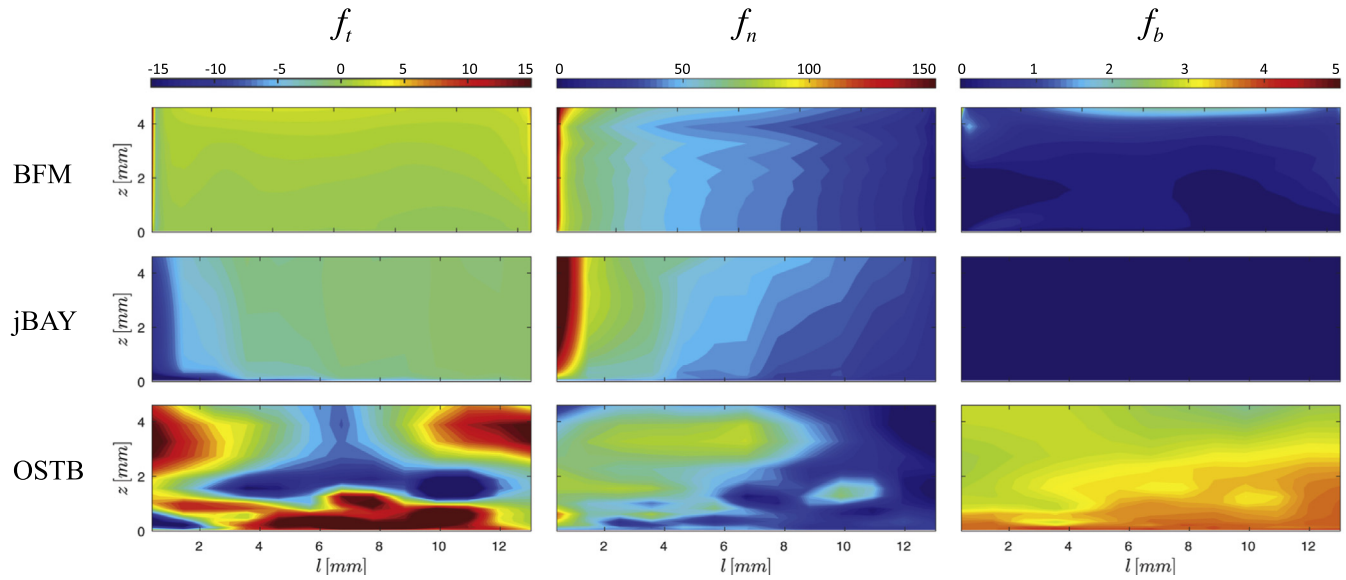

Fig. 14. VG surface force (BFM) and the added body forces for the jBAY and OSTB simulations in tangential, normal and VG spanwise direction. The distributions show the force per unit area, which for the jBAY and OSTB result are obtained by interpolation of the source term to the virtual VG plane (VG pair, mesh M1).

the vortex. Thereby the OSTB approach is a particularly useful tool in a study of the jBAY model, as it allows assessment of both the maximal attainable accuracy on a given mesh and the key features of the corresponding source term.

In Section 5 it is shown that in general the OSTA results show the closest agreement with the objective flow fields, but that the difference with OSTB is small. This indicates that it indeed suffices to add a source term to only a small number of cells in order to generate the desired streamwise vortex, with an appropriate choice for Ω_{VG} defined by the cells that correspond to the physical VG location, similar to the jBAY model. Our results therefore demonstrate that even on a coarse mesh, with a resolution too low to resolve the detailed flow patterns related to vortex creation, there exists a specific driving force that yields an accurate representation of the desired flow field. This is a favorable outcome, as it demonstrates the validity behind the jBAY rationale. Furthermore, selection method B in theory simplifies the analysis and description of the optimal source term due to the possibility of choosing Ω_{VG} as a 2D plane rather than a 3D volume.

Whereas the jBAY model is observed to be unable to accurately represent the shape factor, our OSTB results display a largely improved accuracy in this respect. These results suggest that an improvement for the jBAY model is both desired and possible. It is therefore worthwhile to investigate the differences in the applied source term for both these simulation approaches. For this purpose first the resultant source term is considered, the magnitude and direction of which are visualized in Fig. 13. As expected, it follows that the OSTB source term adds a resultant forcing that is nicely aligned with the exact VG surface force (as extracted from the BFM simulation). The direction of the forcing included by the jBAY model, however, is tilted upstream and downward (as was also observed in [14]). Counter-intuitively, the magnitude of the optimal source term is smaller than the exact VG surface force. This suggest that aiming for an exact representation of the resultant VG surface force is not the optimal approach when using an under-resolved mesh. Indeed, this is confirmed by the source-term distributions, show in Fig. 14 for the VG pair using mesh M1, which are interpolated to the virtual VG plane and displayed as force per unit surface. The jBAY model clearly aims to represent the actual VG force distribution, with the focus being on the leading edge of the VG. The OSTB result on the other hand shows a more uniform distribution of the normal force ($\mathbf{f}_n$), which is less focused on the leading-edge region but spread over the front half of the virtual VG plane. Furthermore, large differences are observed in the secondary components $\mathbf{f}_t$ and $\mathbf{f}_b$, in the tangential and VG-spanwise directions respectively. Although insufficient to draw general conclusions regarding the optimal source term lay-out, the presented results show that aiming for an exact representation of the VG surface force distribution seems not to be the optimal approach for coarse meshes.

8. Conclusion

In this work we optimized the source term added to a CFD simulation in order to represent the flow effects induced by the presence of VGs. Our results prove the viability of the idea to replace a physical obstacle by a local source term, for the situation of an incompressible flow over a flat plate with rectangular, vane-type VGs. It is shown that, even on a low-resolution mesh, a nearly perfect representation of the boundary layer can be achieved when only adding a source term to a limited number of cells in the neighborhood of the VG location. A distinction is made between source terms added in a region surrounding the VG and thereby imposing a specific vortex profile, and source terms added at exactly the VG location that aim to introduce a suitable driving force to initiate vortex creation. Although the rationale between these approaches differs, they both prove to be effective, with the first approach showing the largest accuracy potential.

The presented optimization approach allows determination of the source term which yields the highest accuracy that can potentially be achieved with a source term method on a given (coarse) mesh. It can therefore be used (i) as a tool for the development of improved VG models, (ii) in order to assess whether or not mesh refinement is required for achieving a specific objective, and (iii) to obtain the specific source term that allows achieving this highly accurate result, even for unconventional VG designs. Apart from an academic point of view, the current method is therefore also expected to be particularly useful for industrial applications involving large VG arrays, as useful information can be obtained by studying the simplified sub-problem of only a single VG.

Finally, comparison with results obtained using the jBAY model indicates that research towards an improvement of the latter model is justified and desired. Our approach can be useful in this endeavor, as it allows to quantify the achievable improvement and to identify the deviations of the jBAY source term from the optimal one.

Acknowledgements

This work has received funding from the European Union Seventh Programme for research, technological development and demonstration under grant agreement No. FP7-ENERGY-2013-1/No. 608396 Advanced Aerodynamic Tools for Large Rotors (AVATAR).

References

[1] Gad-el Hak M. Flow control: passive, active, and reactive flow management. Cambridge University Press; 2000.
[2] Lin JC. Review of research on low-profile vortex generators to control boundary-layer separation. Prog Aerosp Sci 2002;38(4–5):389–420. doi:10.1016/S0376-0421(02)00010-6.
[3] Schubauer G, Spangenberg W. Forced mixing in boundary layers. J Fluid Mech 1960;8:10–32.
[4] Miller G. Comparative performance tests on the Mod-2 2.5MW wind turbine with and without vortex generators. Tech. Rep.; 1995. N95-27978.
[5] van Rooij RPJOM, Timmer WA. Roughness sensitivity considerations for thick rotor blade airfoils. In: ASME 2003 wind energy symp., 125; 2003. p. 468–78. ISBN 1-56347-594-4. doi:10.1115/1.1624614.
[6] Gyatt G. Development and testing of vortex generators for small horizontal axis wind turbines. Tech. Rep.; 1986 http://www.osti.gov/energycitations/product.biblio.jsp?osti_id=6801076.
[7] Booker C, Zhang X, Chernyshenko S. Large-scale source term modelling of vortex generation. 27th AIAA appl. aerodyn. conf. San Antonio, Texas; 2009 http://eprints.soton.ac.uk/148655/.
[8] Dudek JC. An Empirical Model for Vane-Type Vortex Generators in a Navier-Stokes Code. AIAA J 2005:1–24. doi:10.2514/1.20141. http://hdl.handle.net/2060/20050080751.
[9] May N. A new vortex generator model for use in complex configuration CFD solvers. In: 19th AIAA Appl. Aerodyn. Conf. Reston, Virigina: American Institute of Aeronautics and Astronautics; 2001. doi: 10.2514/6.2001-2434.
[10] Törnblom O, Johansson AV. A reynolds stress closure description of separation control with vortex generators in a plane asymmetric diffuser. Phys Fluids 2007;19(11). doi:10.1063/1.2800877.
[11] Bender EE, Anderson BH, Yagle PJ. Vortex generator modeling for Navier-Stokes codes. In: 3rd Jt. ASME/JSME fluids eng. conf. San Francisco, CA; 1999. p. 1–7. ISBN 0791819612. doi: FEDSM99-6919.
[12] Wallin F, Eriksson L-E. A tuning-free body-force vortex generator model. In: 44th AIAA aerosp. sci. meet. exhib. Reston, Virigina: American institute of aeronautics and astronautics; 2006. p. 1–12. doi:10.2514/6.2006-873. ISBN 978-1-62410-039-0.
[13] Jirasek A. Vortex-Generator model and its application to flow control. J Aircr 2005;42(6):1486–91. doi:10.2514/1.12220.
[14] Florentie L, van Zuijlen AH, Hulshoff SJ, Bijl H. Effectiveness of side force models for flow simulations downstream of vortex generators. AIAA J 2017;55(4):1373–84. doi:10.2514/1.J055268.
[15] Othmer C. A continuous adjoint formulation for the computation of topological and surface sensitivities of ducted flows. Int J Numer Methods Fluids 2008;58(8):861–77. doi:10.1002/fld.1770.
[16] Zymaris AS, Papadimitriou DI, Giannakoglou KC, Othmer C. Continuous adjoint approach to the spalart-Allmaras turbulence model for incompressible flows. Comput Fluids 2009;38(8):1528–38. doi:10.1016/j.compfluid.2008.12.006.
[17] Holm DD. Taylor'S hypothesis , Hamilton's principle, and the LANS-a model for computing turbulence. Los Alamos Sci 2005(29):172–80.
[18] Dwight RP, Brezillon J. Effect of approximations of the discrete adjoint on gradient-Based optimization. AIAA J 2006;44(12):3022–31. doi:10.2514/1.21744.
[19] Schulz V, Gherman I. One-Shot methods for aerodynamic shape optimization. In: Notes numer. fluid mech. multidiscip. des. Springer, Berlin, Heidelberg; 2009. p. 207–20. http://link.springer.com/10.1007/978-3-642-04093-1_15.
[20] Srinath DN, Mittal S. An adjoint method for shape optimization in unsteady viscous flows. J Comput Phys 2010;229(6):1994–2008. doi:10.1016/j.jcp.2009.11.019.
[21] Nita C, Vandewalle S, Meyers J. On the efficiency of gradient based optimization algorithms for DNS-based optimal control in a turbulent channel flow. Comput Fluids 2016;125:11–24. doi:10.1016/j.compfluid.2015.10.019. http://linkinghub.elsevier.com/retrieve/pii/S004579301500359X.
[22] Nocedal J, Wright SJ. Numerical optimization. Second; 2006. ISBN 978-0-387-40065-5.
[23] Steihaug T. The conjugate gradient method and trust regions in large scale optimization. SIAM J Numer Anal 1983;20(3):626–37. doi:10.1137/0720042.
[24] Yao C, Lin J, Allan B. Flow-field measurement of device-induced embedded streamwise vortex on a flat plate. In: NASA STI/recon tech. rep. ...; 2002. p. 16. ISBN 9781624101052. doi:10.2514/6.2002-3162.
[25] Baldacchino D, Ragni D, Simao Ferreira C, van Bussel G. Towards integral boundary layer modelling of vane-type vortex generators. 45th AIAA fluid dyn. conf. Reston, Virginia: American institute of aeronautics and astronautics; 2015 http://www.lr.tudelft.nl/fileadmin/Faculteit/LR/Organisatie/Afdelingen_en_Leerstoelen/Afdeling_AEWE/Wind_Energy/Research/Publications/Publications_2015/Towards_integral_boundary_layer_modelling_of_vane-type_vortes_generators.pdf. doi:10.2514/6.2015-3345. ISBN 978-1-62410-362-9.